Oscillations of electrical potential along a root of a higher plant

K. Toko, M. Souda, T. Matsuno, and K. Yamafuji
Department of Electronics, Faculty of Engineering, Kyushu University 36, Fukuoka 812, Japan

ABSTRACT Higher plants exhibit an oscillation of electrical potential near the surface along the root. The oscillation was studied with the aid of both the usual intracellular microelectrode technique and the extracellular multielectrode technique, the latter making it possible to measure simultaneously electrical potentials along the root. It was found that the oscillation of extracellular surface potential showed the largest amplitude in the elongation region, and the phase of the oscillation in this region differed by 180 degrees from that in the mature region, where the oscillation appeared coherent. The measurement of the intracellular electrical potential suggested the existence of oscillatory components localized to the parenchyma/xylem interface in the elongation region. A theoretical analysis based on an electrical circuit network described the above-mentioned behavior. It was shown that the oscillation was propagated along the root over several centimeters without substantial decay in the mature region.

INTRODUCTION

Rhythmic oscillations of electrical potential appear near the surfaces of roots of higher plants (Scott, 1957; Jenkinson and Scott, 1961). This kind of oscillation in a multicellular biological system may be a property of dissipative structures appearing far from equilibrium. A typical example may be the Belousov-Zhabotinskii reaction in chemical reaction systems coupled with chemical diffusion (Nicolis and Prigogine, 1977; Krinsky and Agladze, 1983), where sequential circular or spiral waves of products are generated spontaneously.

The oscillation of the electrical potential near the root surface in the elongation region differs by 180 degrees in phase from that in the mature region (Jenkinson and Scott, 1961; Toko et al., 1986). It appears coherent in the mature region over several centimeters (Toko et al., 1986; Hayashi et al., 1987). The mechanism that underlies this behavior, however, has not been elucidated.

In the present paper, we studied the spatial properties of the electrical oscillation in the roots of higher plants with intracellular microelectrode techniques (Bowling, 1972) and with extracellular multielectrodes (Toko et al., 1986; Toko and Yamafuji, 1988). It was suggested that the oscillation arises from the parenchyma/xylem interface in the elongation region and is propagated along the xylem inside the root to the mature region. A theoretical calculation based on an electrical circuit network model explained the observed oscillations of the membrane electrical potentials and the surface electrical potentials in the elongation and mature regions.

MATERIALS AND METHODS

Fig. 1 shows an experimental setup. The measuring system is composed of 64 channels for electrodes, a handmade electrical circuit, and a personal computer. Roots of the germinating hypogeal plant (adzuki: *Phaseolus chrysanthos*) with first true leaves were used. Experimental details are similar to those previously described (Toko et al., 1986, 1987; Yoshida et al., 1988). The 4–7-d-old root was laid horizontally in 0.1 mM KCl and 0.05 mM $CaCl_2$ in the chamber. The spatial pattern of the extracellular electrical potential V_S was measured by arranging ~10–30 pipette electrodes near the root surface with ~1.5-mm intervals. Each electrode has a tip diameter of ~300 μm and is filled with 100 mM KCl and 1% agar, containing an Ag/AgCl wire.

A 25-cm-long Ag/AgCl wire as a reference electrode was placed within the agar containing 100 mM KCl solution parallel with the root distant by 5 cm so that the electrical potential might decay to zero on the average at the reference point. The aqueous phase surrounding a root was separated from the agar using a plastic shield with a 1-mm-wide slit so as to decrease KCl diffusion into the aqueous phase. The extracellular electrical potential near the root surface did not decay with time during experiments, and hence the ion concentration is considered to have scarcely changed; the extracellular potential would have decreased due to the increase in conductance, if the concentration had increased. Because the time required for scanning over 20 electrodes is only 1 s, the dynamic change in electrical potentials in the root was easily measured. The power spectrum was calculated by means of a maximum entropy method.

The intracellular electrical potential within the root V_P was measured simultaneously with microelectrodes (Bowling, 1972; Katou, 1978; Behrens and Gradmann, 1985); the zero point of the electrical potential was taken to be the position of the above reference electrode. Two electrodes were inserted into the root at points of 4 and 25 mm from the root tip. The 4-mm point corresponds to the elongation region, which lies between 2 and 5 mm from the root tip, the 25-mm point corresponding to the fully-grown mature region, which extends over the remaining part except for the root cap. The microelectrode tip was inserted to the cell vacuole in cortex at ~200 μm depth, where the potential was almost

0006-3495/90/02/269/11 $2.00

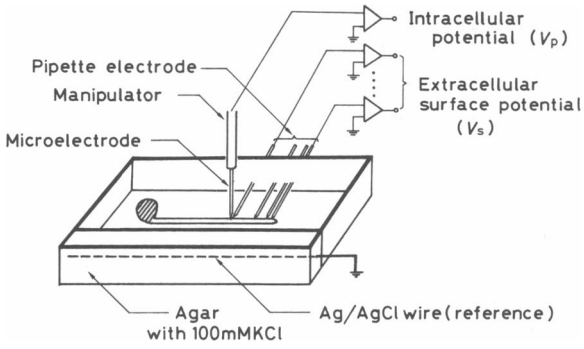

FIGURE 1 Experimental setup. A root was placed horizontally on three filter papers in the chamber with 0.1 mM KCl + 0.05 mM $CaCl_2$ solution. Pipette electrodes were fixed by an agar plate at 1.5 mm intervals near the root surface. Microelectrodes were positioned by a micromanipulator. The reference electrode, a 25-cm-long Ag/AgCl wire, was placed in an agar block containing 100 mM KCl far from the root. The intracellular potential V_P and the extracellular surface potential V_S were measured with the reference electrode as the origin of electrical potential. The membrane potential is defined by $V_P - V_S$. In some cases, air or nitrogen gas was led into the tightly closed chamber.

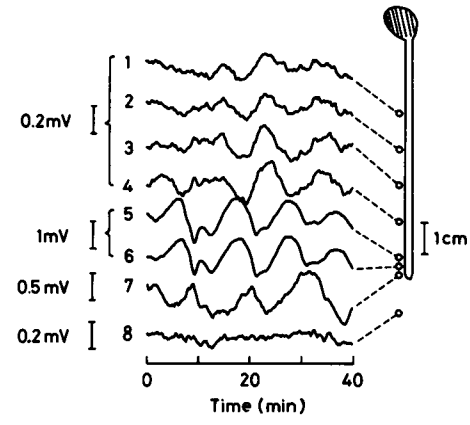

FIGURE 2 Oscillations of extracellular electrical potentials at eight points for a root 89 mm long. The scale is attached to each curve. Oscillations were not observed in the aqueous medium. Oscillations in the elongation region were 180-degrees out-of-phase from those in the mature region.

constant radially, as previously reported (Bowling, 1972; Ginsburg and Ginzburg, 1974). The membrane potential is defined as the intracellular potential minus the surface potential, i.e., equal to $V_P - V_S$.

The experiments were performed at 28 ± 2°C. In some cases, nitrogen or air was allowed to flow at a controlled rate into a tightly closed chamber to get additional information on the spatial characteristics of oscillations.

EXTRACELLULAR ELECTRICAL OSCILLATIONS

Fig. 2 shows a typical example of the electrical potentials in the aqueous solution near the surface of a root, 89 mm in length. Electrode 8 was placed 10 mm distant from the root; electrode 7 was located at the root cap. The electrical potential in the elongation zone was measured by two electrodes 5 and 6 with the mature region by 1 to 4. The potential oscillated along the root surface, but the amplitude was flattened distant from the root. The oscillation was apparently coherent in the mature region and its phase differed by 180 degrees from that in the elongation region. The amplitude of oscillation was largest in the elongation region, whereas it was usually small in the mature region. At the boundary between the elongation region and the mature region, the oscillation was obscure in many cases. In some cases, however, the phase appeared to change continuously from the elongation region to the mature region (Hayashi et al., 1987).

The coherent property in the mature region was always found when the root showed the electrical oscillation. While the experiments were done with about 350 roots, oscillations were found in about 200 roots. In our experience, it seems that the roots showing no oscillations had relatively slow growth speed. In fact, the oscillations scarcely appeared at temperatures as low as 15°C.

The fact that the electrical potential oscillated with the largest amplitude in the elongation region may suggest the existence of an oscillatory origin in this region. Fig. 3 *a* may confirm this suggestion, where 30 electrodes were arranged at 1.7-mm intervals from the tip of a root 75 mm in length. The electrical potential oscillated with different frequencies within the elongation region. A relative scale was adopted to make clearer the phase relation in the mature region. Whereas complete coherency was lacking, the same-phase behavior was found over 20 mm in some periods, e.g., at electrodes 1 ~ 10 between 1.2 and 1.6 h. Large-amplitude oscillations appeared at electrodes 26 ~ 30 located in the meristem and the elongation zone. At the boundary between the elongation region and the mature region (electrode 25), the oscillation was fairly obscure. The phase at electrode 26 in the rear part of the elongation region differed by 180 degrees from that at electrode 24 in the front part of the mature region. This tendency was observed in many roots.

Fig. 3 *b* shows the power spectrum of the oscillations at electrode numbers 1, 5, 17, 22, 27, and 29. At electrodes 1–22, in the mature region, the spectrum peaks around a frequency of 0.0012 Hz, the period of oscillation being 13.8 min, although other frequency components coexist in some places, e.g., at electrode 17. It should be noted that electrode 27 located at the rear part of the elongation region shows the same frequency as that in the mature region. But electrode 29 located at the front part of the elongation region shows a different frequency, i.e., 0.0016

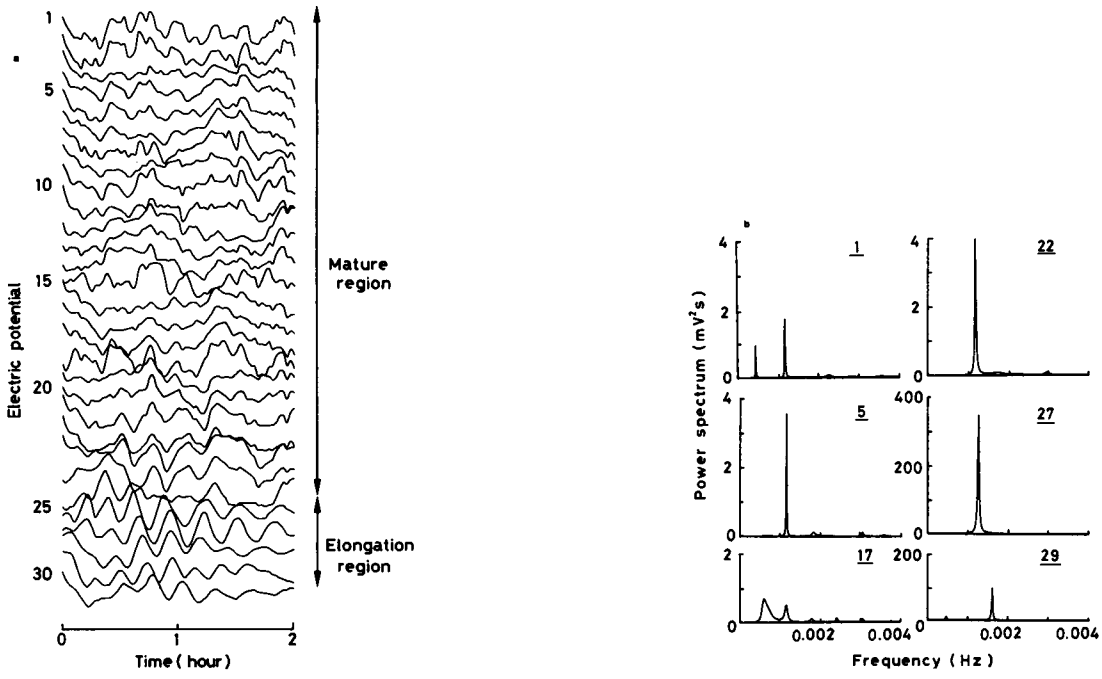

FIGURE 3 Oscillations of extracellular electrical potentials along the root surface after replacement of N_2 gas by air (*a*) and power spectra vs. frequency (*b*). The root was pretreated with N_2 gas for 2 h. (*a*) The data of arbitrary scales at 30 electrodes are arranged from the basal part to the tip with the abscissa indicating time. Electrodes were arranged at 1.7-mm intervals from the root tip for a 52-mm distance along the root. (*b*) Power spectra are shown for the electrodes 1, 5, 17, 22, 27, and 29. The electrodes 1 ~ 25 were in the mature region. The elongation region contains electrodes 26–29.

Hz equivalent to the 10.4-min period. These results may imply the existence of a group of oscillators in the elongation region, and furthermore suggest that the oscillatory signal in the rear part of the elongation region is propagated to the front part of the mature region.

Existence of a group of oscillators in the elongation region was found in other examples (e.g., Hayashi et al., 1987). The period of oscillation changed from 6 to 12 min, and then to 18 min, the latter two being integer ratios to 6. This kind of change was also reported for a circadian rhythm (Hoffman, 1969; Hoppensteadt and Keener, 1982), where the behavior was attributed to a group of coupled oscillators.

SURFACE ELECTRICAL POTENTIAL AND MEMBRANE POTENTIAL

Fig. 4 shows the electrical potentials near the surface potential, denoted by dashed lines, and the membrane potential, denoted by solid lines, measured in the elongation region (*a*) and the mature region (*b*) for a root with 54 mm length. The phase of oscillation of the surface electrical potential in the elongation region differed by 180 degrees from that in the mature region, as is the case in Fig. 2. The membrane potential and also the intracellular potential in the elongation region oscillated with nearly the same phase as the surface electrical potential in this region. It suggests that the membrane at the surface did not itself generate the electrical oscillation. If the membrane electrical element had oscillatory behavior, the electrical potentials at both sides of the membrane should always have oscillations out of phase with each other. This can be understood from a simple consideration: If the electrical potential at one side changes by ΔV, then that at another side changes by $-\Delta V$, because the direction of electrical current is opposite when observed from the midpoint of the element. The mature region, on the other hand, did not show the oscillation of the membrane potential, because the intracellular potential oscillated with the same magnitude as the surface electrical potential. In other words, the intracellular potential in the mature region oscillated with a 180-degree different phase from the surface electrical potential in the elongation region.

From these results, it can be concluded that the oscillatory components do not exist within the surface membrane. As is well known, the parenchyma symplast behaves as an electrical continuum with equipotential

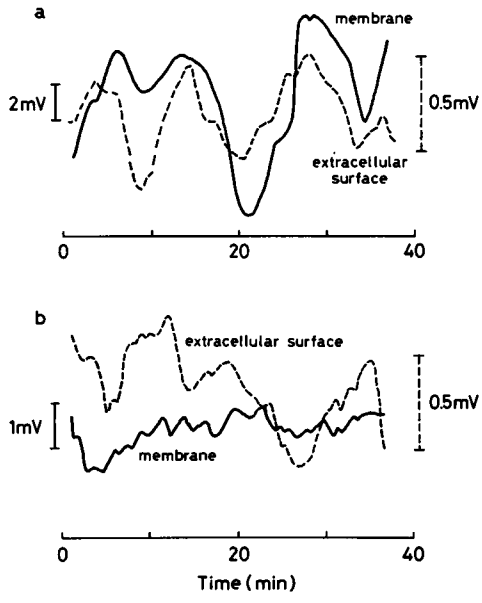

FIGURE 4 Extracellular surface electrical potentials (---) and membrane potentials (——) in the elongation region (*a*) and the mature region (*b*). The surface potential in the elongation region oscillated 180 degrees out-of-phase from that in the mature region. Whereas the elongation region showed oscillation of the membrane potential, the mature region did not. In the mature region, the change of the surface electrical potential was the same as that of the intracellular potential.

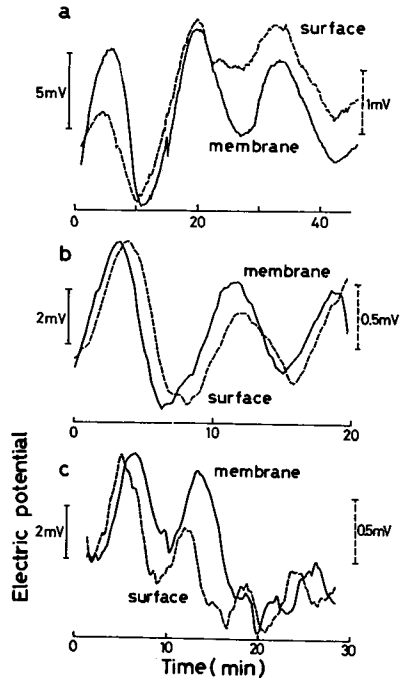

FIGURE 5 Three examples of relations between the membrane potential (——) and the surface electrical potential (---) in the elongation region observed in different roots. (*a*) The electrical potentials oscillated with the same phase; (*b*) the membrane potential was slightly advanced; (*c*) the surface potential was slightly advanced.

level (Arisz, 1956; Bowling, 1972; Katou, 1978). Ion channels and pumps existing at two interfaces are therefore important for the generation of electrical potentials (Spanswick, 1981). One interface is between the root surface and the parenchyma, and another is between the xylem and the parenchyma (Hanson, 1978; de Boer et al., 1983). Together with the results in Figs. 2 and 3, this suggests that the oscillation arises from the periodic change in the electrical potential across electrical elements at the xylem/parenchyma interface in the elongation region. Furthermore, the oscillation is not propagated along the parenchyma/surface interface, i.e., the epidermal cell membrane, because the membrane potential did not oscillate in the mature region in spite of the oscillation of the extracellular surface potential. The electrical potential would, therefore, appear to be propagated inside the parenchyma symplast along the xylem/parenchyma interface.

Fig. 5 shows three examples of the phase relation between the surface electrical potential and the membrane potential in the elongation region using different roots. The oscillations in Fig. 5 *a* showed the same phase. While the membrane potential was slightly advanced in phase compared with the surface potential in Fig. 5 *b*, the opposite relation was found in Fig. 5 *c*. The difference of the phase between the surface potential and the membrane potential may reflect a slight contribution of the surface/parenchyma interface to the oscillation. If the electrical potential generated purely by the electrical elements at this interface oscillates weakly in a different phase from that at the xylem/parenchyma interface, the resulting surface potential may oscillate by the different phase from the membrane potential.

THEORY

In the first part of the present section, the distance over which the electrical potential change extends is calculated with the aid of an electrical circuit network model of the electrophysiological structure. The second part is concerned with modeling oscillations of surface electrical potentials and intracellular potentials to explain the experimental results.

Propagation of electrical potential along a root

Fig. 6 gives a theoretical model of an electrical circuit network of a root in an aqueous solution. In the longitudi-

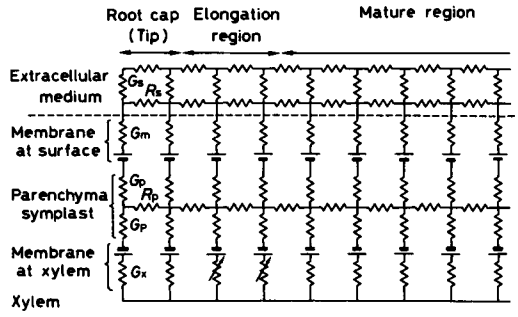

FIGURE 6 A theoretical model for expressing the flow of electrical current along and around a root. Because the parenchyma behaves as an electrical continuum with high conductivity, the generation of electrical potential is mainly dominated by the membrane electromotive forces and electrical resistances existing at the two interfaces of surface/parenchyma and xylem/parenchyma. The electrical resistance at xylem/parenchyma interface in the elongation region is assumed to oscillate.

nal direction, the electrical circuit is composed mainly of three parts belonging to the root cap, the elongation region, and the mature region. In the radial direction, electrophysiological results suggest that there are five regions (Arisz, 1956; Bowling, 1972; Katou, 1978; de Boer et al., 1983; Bacic and Ratkovic, 1984), i.e., the external aqueous solution, the plasmalemma of epidermal and cortical cells, the parenchyma symplast, the membrane at the xylem/parenchyma interface, and the xylem.

The external aqueous solution is modeled by a network of electrical resistances. The plasmalemma of epidermal and cortical cells corresponds to the membrane at the root surface, which is modeled by a membrane electromotive force and a membrane electrical resistance. These electrical elements come from incorporation of those for expressing electrogenic properties of ion channels and ion pumps (Hodgkin and Huxley, 1952; Hanson, 1978; de Boer et al., 1983; Toko et al., 1989). The electrical properties of the parenchyma symplast are treated by an equivalent network of electrical resistances. The membrane at the xylem/parenchyma interface at any point is modeled by a series circuit of a membrane electromotive force and a membrane electrical resistance. The potential inside the xylem is assumed to be homogeneous in the longitudinal direction (Ichino et al., 1973), because the ion concentrations are as high as a few tens of millimolar (Bowling, 1976).

Let us consider the propagation of electrical potential change in the longitudinal direction of a root. As shown in the Appendix, we can safely assume two independent pathways along the root. The first is the propagation along the surface/parenchyma interface, and the second is along the xylem/parenchyma interface. Let V_1 and V_2 denote the potential differences across these two interfaces, respectively (see also Fig. A1), which are characterized by space constants λ_1 and λ_2:

$$\Delta V_i = \Delta V_{i0} \exp(-x/\lambda_i) \qquad \text{with i = 1 and 2,} \qquad (1)$$

where ΔV_i is the electrical potential change as a function of x, and ΔV_{i0} expresses a change induced at $x = 0$, where x denotes the longitudinal spatial coordinate. Because the computed propagation velocity is much faster than the period of the oscillation (see Appendix), the time scale considered in derivation of Eq. 1 can be ignored in discussing the oscillation. The space constants were estimated to be $\lambda_1 = 3.0$ mm and $\lambda_2 = 70$ mm (Appendix). This result shows that the electrical oscillation will decay within a short distance along the surface/parenchyma interface. The electrical oscillation, on the other hand, along the xylem/parenchyma interface extends over several centimeters.

This result agrees with the observation in Fig. 4 that the membrane potential did not oscillate in the mature region while it oscillated in the elongation region. The oscillation of membrane electrical potential in the elongation region decays within a few millimeters. The oscillation of the surface electrical potential in the mature region arises from oscillation in the intracellular medium, which is propagated from the elongation region along the xylem/parenchyma interface.

Relation between surface electrical potentials in elongation and mature regions

Let us simplify the theoretical model in Fig. 6 by dividing the longitudinal direction into three regions, assuming electrical homogeneity in each region: the root cap, the elongation region, and the front part of the mature region. In Fig. 7, the symbols (T), (E), and (M) are attached, respectively, to the electrical elements belonging to these regions. The electromotive force and the electrical resistance of the membrane is denoted by E_i and r_i, respectively, with i equal to 1 or 2, corresponding to the quantities at the plasmalemma of epidermal cells or those at the xylem/parenchyma interface, respectively. The longitudinal resistance of parenchyma symplast between the root cap and the elongation region is expressed by $R_P^{(TE)}$, and that between the elongation and the mature regions is $R_P^{(EM)}$. The longitudinal resistances in the aqueous solution are $R_S^{(TE)}$ and $R_S^{(EM)}$. The electrical potential at each point is denoted by V with the subscripts s, p, and x implying the surface, the parenchyma symplast and the xylem, respectively.

The electrical resistances between the surface regions and the reference electrode are denoted by $R_r^{(T)}$, $R_r^{(E)}$, and

$R_r^{(M)}$:

$$R_r^{(i)} = \frac{1/L^{(i)}}{1/L^{(T)} + 1/L^{(E)} + 1/L^{(M)}} R_r \text{ with i = T, E, and M, (2)}$$

where $L^{(i)}$ is the length of each region and R_r is the sum of the electrical resistances $R_r^{(T)}$, $R_r^{(E)}$, and $R_r^{(M)}$, which should be set to infinity, because the electrical current flowing into the reference electrode is zero. Eq. 2 can be easily checked by noticing that R_r is equal to $(L^{(T)-1} + L^{(E)-1} + L^{(M)-1})R$, with R denoting a resistance per unit length (Ω cm).

Let us define the loop electrical currents i_1 to i_4 as indicated in Fig. 7. Using elementary circuit theory (e.g., Floyd, 1989), it is easy to show that they obey the following equations:

$$AI = E, \tag{3}$$

where the matrix A is defined by

$$A = \begin{pmatrix} a_{11} & -a_{12} & 0 & -a_{14} \\ -a_{12} & a_{22} & -a_{23} & 0 \\ 0 & -a_{23} & a_{33} & -a_{34} \\ -a_{14} & 0 & -a_{34} & a_{44} \end{pmatrix}, \tag{4}$$

with I and E denoting the transpose vectors of (i_1, i_2, i_3, i_4) and (E_1, E_2, E_3, E_4), respectively. The quantities a_{ij} and E_i are given by

$$\begin{aligned} &a_{11} = r_1^{(E)} + r_1^{(M)} + R_S^{(EM)} + R_P^{(EM)}, a_{12} = r_1^{(E)}, \\ &a_{14} = R_P^{(EM)}, a_{22} = r_1^{(E)} + r_1^{(T)} + R_S^{(TE)} + R_P^{(TE)}, \\ &a_{23} = R_P^{(TE)}, a_{34} = r_2^{(E)}, a_{33} = r_2^{(E)} + r_2^{(T)} + R_P^{(TE)}, \\ &a_{44} = r_2^{(E)} + r_2^{(M)} + R_P^{(EM)}, E_1 = E_1^{(M)} - E_1^{(E)}, \\ &E_2 = E_1^{(E)} - E_1^{(T)}, E_3 = E_2^{(T)} - E_2^{(E)}, \\ &E_4 = E_2^{(E)} - E_2^{(M)}. \end{aligned} \tag{5}$$

Eqs. 3 with Eqs. 4 and 5 give the loop electrical currents i_1 to i_4. As already discussed, the electrical model of the membrane at the xylem/parenchyma in the elongation region shows oscillatory behavior. Here we assume for simplicity that the electrical resistance $r_2^{(E)}$ oscillates although $E_2^{(E)}$ may also oscillate in real cases. Because we are now interested in the phase relation of electrical potentials between the elongation and the mature regions, this simplification causes no serious error. The following variation of $r_2^{(E)}$ is assumed:

$$r_2^{(E)} = A[1 + \sin(2\pi t/\tau)], \tag{6}$$

where A and τ are numerical parameters for the amplitude and the period of oscillation, respectively, with t denoting the time.

The electrical potentials also can be obtained from

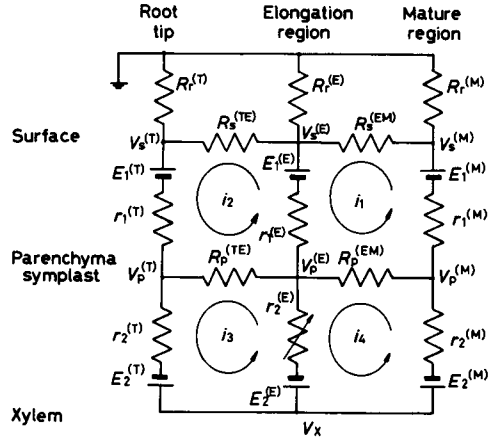

FIGURE 7 A simplified model for calculating the electrical potentials in the root cap and meristem region, the elongation region, and the front part of the mature region, limited to ~10 mm length from the root tip. The lengths of the root tip, the elongation and the mature reigons are 1, 5, and 4 mm, respectively.

Kirchhoff's laws and are given by

$$\begin{aligned} V_S^{(E)} &= (L^{(T)}R_S^{(TE)}i_2 - L^{(M)}R_S^{(EM)}i_1)/L \\ V_P^{(M)} &= V_S^{(E)} + (r_1^{(M)} + R_S^{(EM)})i_1 - E_1^{(M)}, \end{aligned} \tag{7}$$

and so on. In Eq. 7, L is the total length equal to $L^{(T)} + L^{(E)} + L^{(M)}$.

Fig. 8 shows the calculated results of the extracellular

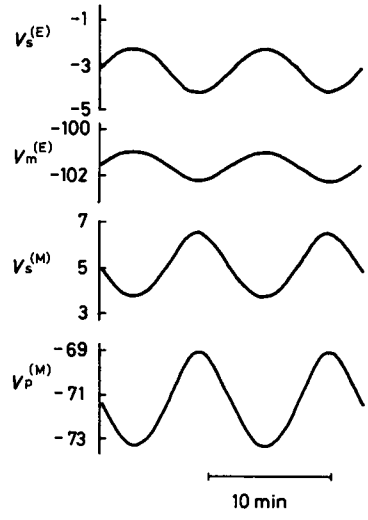

FIGURE 8 Theoretical calculation of the surface electrical potential $V_S^{(E)}$ and the membrane potential $V_m^{(E)}$ in the elongation region and the surface potential $V_S^{(M)}$ and the intracellular potential $V_P^{(M)}$ in the front part of the mature region. Potentials are in millivolts. The membrane electrical resistance in the elongation region is assumed to oscillate at the xylem/parenchyma interface, as expressed by Eq. 6.

surface electrical potential in the elongation region $V_S^{(E)}$, the membrane potential $V_m^{(E)}$, the surface potential in the front part of the mature region $V_S^{(M)}$, and the intracellular electrical potential $V_S^{(M)}$. The values adopted for $R_S^{(TE)}$, $R_S^{(EM)}$, $r_1^{(M)}$, etc., are given in the Appendix. The surface potential $V_S^{(E)}$ oscillates with the same phase as the membrane potential $V_m^{(E)}$, which explains the experimental observation in Fig. 4. The phase of the intracellular electrical potential $V_P^{(M)}$ differs by 180 degrees from that of the above two.

Because the electrical potential decays along the root at the surface/parenchyma interface, $V_S^{(E)}$ and $V_S^{(M)}$ decay around the elongation region and do not reach the entire mature region over several centimeters. Instead, the large value of λ_2 in Eq. 1 suggests that the electrical potential $V_P^{(M)}$ inside the root in the front part of mature region can be propagated along the xylem/parenchyma interface. It appears at the whole extracellular surface of the mature region because the ion fluxes across the membrane are nearly steady state, as can be understood from Fig. 4, where the membrane potential does not oscillate.

The propagation speed at the xylem/parenchyma interface is estimated to be on the order of 10 cm/s (see Appendix); thus the apparent coherence of the surface electrical potential is observed in the mature region, and its phase differs by 180 degrees from the elongation region. In this way, the experimental results have been explained by assuming an oscillation of the electrical resistance of the membrane at the xylem/parenchyma interface. When we assumed that the oscillation of electrical resistance occurred at the surface side of the membrane, the surface electrical potential $V_S^{(E)}$ oscillated out of phase with the membrane potential $V_m^{(E)}$, in contradiction to the experimental results in Fig. 4.

DISCUSSION

Phase relation and propagation

In Fig. 9, a theoretical model for explaining the present experimental observations is illustrated. An electrical current loop is formed around the elongation region through the variation in the value of electrical elements, e.g., the membrane electrical resistance at the xylem/parenchyma interface. This process leads to the out of phase relationship between the surface electrical potentials of the elongation region and the front part of the mature region. But the electrical potential in the front part of the mature region decays at once, and hence it is not propagated to the entire mature region. Instead, the electrical change produced in the parenchyma symplast is propagated to the mature region along the xylem/parenchyma interface. This change is measured as that in the extracellular surface potential emerging across the

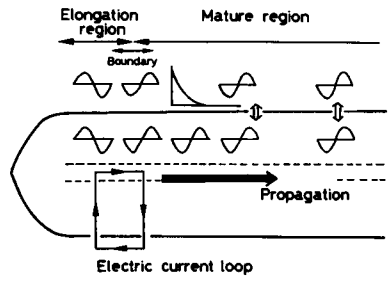

FIGURE 9 Schematic illustration of oscillations of electrical potentials in a root. Only the phase relation is shown by ∿, and a curve depicted in the mature region implies the fast decay of electrical oscillations. In the elongation region, the membrane potential V_m shows similar behavior to the intracellular potential V_P because of the definition of $V_m = V_P - V_S$, where the change of V_P is larger than that of V_S. In the mature region, the change of V_S is the same as that of V_P; hence V_m does not oscillate.

membrane at the surface side apparently coherent over the mature region. Because the above change in the parenchyma of the mature region has an out-of-phase relation with the surface electrical potential in the elongation region, the extracellular surface potentials differ by 180 degrees in the elongation and the mature regions.

The simplified theoretical model in Fig. 7 is related to the far-from-equilibrium region at the root tip side containing the front part of the mature region. The membrane potential, therefore, is not the same as that in the fully-grown mature region, where the surface and the parenchyma are nearly balanced electrochemically with each other. Although it was shown theoretically that the membrane potential oscillates in the front part of the mature region, the measurement is difficult because this boundary region showed obscure oscillations, as in Fig. 3 *a*.

Let us discuss the theoretical result in Fig. 8, where the surface electrical potential $V_S^{(E)}$ in the elongation region oscillates by 180 degrees out of phase with the intracellular potential $V_P^{(M)}$ in the front part of the mature region. The out-of-phase relationship can be expressed by a mathematical relation where the temporal change in $V_S^{(E)}$ has an opposite sign from that in $V_P^{(M)}$. From Eq. 3, we can calculate the linear response in the first two loop currents, Δi_1 and Δi_2, due to a change in $r_2^{(E)}$, $\Delta r_2^{(E)}$:

$$\Delta i_1 = (v_1 r - w_1 q)\Delta r_2^{(E)}/r^2$$
$$\Delta i_2 = (v_2 r - w_2 q)\Delta r_2^{(E)}/r^2, \quad (8)$$

where q, r, v_1, w_1, v_2, and w_2 are defined in the Appendix.

Substitution of Eq. 8 into Eq. 7 gives the temporal changes in $V_S^{(E)}$ and $V_P^{(M)}$:

$$\Delta V_S^{(E)} = \alpha_S \Delta r_2^{(E)}$$
$$\Delta V_P^{(M)} = \alpha_P \Delta r_2^{(E)}, \quad (9)$$

where α_S and α_P are defined by

$$\alpha_S = [L^{(T)}R_S^{(TE)}(v_2r - w_2q) - L^{(M)}R_S^{(EM)}(v_1r - w_1q)]/Lr^2$$
$$\alpha_P = \{L^{(T)}R_S^{(TE)}(v_2r - w_2q) + [(L - L^{(M)})R_S^{(EM)} + Lr_1^{(M)}](v_1r - w_1q)\}/Lr^2. \quad (10)$$

The first terms originate from Δi_2, the second being due to Δi_1. Calculation of the ratio $\Delta i_1/\Delta i_2 = (v_1r - w_1q)/(v_2r - w_2q)$ gives -5.6. Thus Δi_1 is larger than Δi_2, and decreases when Δi_2 increases.

Because the ratio of $L^{(T)}R_S^{(TE)}$ to $L^{(M)}R_S^{(EM)}$ is ~0.06, the expressions for α_S and α_P can be simplified to

$$\alpha_S = -L^{(M)}R_S^{(EM)}(v_1r - w_1q)/Lr^2$$
$$\alpha_P = [1 - (1 + r_1^{(M)}/R_S^{(EM)})L/L^{(M)}]\alpha_S. \quad (11)$$

The total length L is, of course, larger than the length of the front part of mature region $L^{(M)}$; hence, α_S and α_P also have opposite sign. We can, therefore, conclude from Eq. 9 that $V_S^{(E)}$ is out of phase with $V_P^{(M)}$, as calculated numerically in Fig. 8.

This result also can be seen in another fashion. Whereas the electrical potential change $\Delta V_S^{(E)}$ of Eq. 9 arises from the difference between contributions of Δi_1 and Δi_2, the result of $\Delta i_1/\Delta i_2 = -5.6$ implies that the effect of i_1 is larger than i_2. This is a consequence of the larger electrical resistances across which the current flows. The electrical potential $V_P^{(M)}$ in Eq. 7 is essentially determined by the sum of $V_S^{(E)}$ and the term involving i_1. Thus effect of i_1 is larger than that of i_2 for both $V_S^{(E)}$ and $V_P^{(M)}$. Using Fig. 7, therefore, we can regard the surface in the elongation region and the parenchyma in the mature region as the sink and the source of electrical current, respectively, when the electrical potential is measured from the reference point. This also leads to the out-of-phase relationship between $V_S^{(E)}$ and $V_P^{(M)}$.

Because $\Delta i_1/\Delta i_2$ is given by Eq. A10 and does not depend on the electromotive forces, the direction of change in electrical current loops is not affected by the existing electrical spatial pattern but is determined by the relative magnitude of electrical resistances, which agrees with Thévenin's theorem (e.g., Floyd, 1989). Because the surface area across which ions flow is smaller in the tip region, $r_1^{(T)}$ in Fig. 7 becomes much larger than $r_1^{(E)}$ and $r_1^{(M)}$. This leads necessarily to $|\Delta i_1| \gg |\Delta i_2|$. From these considerations, it can be concluded that the out-of-phase relationship holds generally between the elongation and the mature regions. The coherent length over which the electrical oscillation appears in the same phase, on the other hand, depends directly on the membrane electrical resistance, as can be seen from λ_2 in Eq. A6. Nevertheless, its dependence is not strong because λ_2 is inversely proportional to the square root of the membrane conductance.

Mechanism and role of oscillations

We have considered two different characteristics in assuming the periodic change in the membrane electrical resistance in the elongation region: one is the large-amplitude oscillation in this region, and another is the coexistence of different frequencies, which suggests a group of weakly coupled oscillators. The oscillation was amplified when a periodic change in pressure was applied to the elongation zone (Jenkinson and Scott, 1961). This result may agree with the present interpretation. Because electrical homogeneity in the elongation region has been assumed for simplicity in Fig. 7, a situation as complicated as that in Fig. 3 cannot be described. In this case, however, it may be sufficient to explain a phenomenon limited to the elongation region, and hence a mathematical treatment may be possible from the viewpoint of coupled oscillators (Hoppensteadt and Keener, 1982).

In Eq. 6, the resistance $r_2^{(E)}$ was assumed to oscillate. Whereas such a membrane conductance change may originate from activity changes in ion pumps and channels, the conductance change must be measured by means of, e.g., a water-film electrode (Ogata, 1983). It is very interesting that the roots showed no oscillations when they had a slow growth speed. A relationship between the oscillation and the growth must be elucidated.

As shown theoretically (Toko et al., 1989), the steady electrical currents around the root are mainly produced by K^+ ions, whereas H^+ contributes to cell wall expansion through acidification. Because oscillations appeared in the absence of Ca^{2+} ions (Toko et al., 1986), the major ion causing the oscillations can be considered to be K^+ in the present experiment. Coupled to flow of K^+ ions, H^+ may also move in the extracellular and intracellular media to affect metabolic activity.

The xylem was approximated to be equipotential in Figs. 6 and 7. Whereas an experiment supporting this assumption has been reported (Ichino et al., 1973), there exists a possibility of a potential gradient along the xylem near the root tip, because a large electrical current flows there. The resulting potential gradient, however, may be small because of the moderate ion concentrations in the xylem vessel (Bowling, 1976). Thus, it does not seriously affect the present theoretical result of the out-of-phase relation. Furthermore, a root contains several xylem vessels. One xylem vessel was taken into account here because they can be treated separately due to the low conductivity of the membrane at the xylem/parenchyma interface.

As the root elongates, the elongation region gradually changes to the mature region. It means conversion of the oscillatory active components into the nonoscillatory passive components. The newly produced elongation region will show an electrically oscillatory behavior. At the

present stage, a mechanism of the oscillation in itself is not clear. Since an applied pressure affected the oscillation (Jenkinson and Scott, 1961), the oscillation is considered to have a relation to the cell expansion leading to the elongation growth.

Oscillations have been observed in many cellular systems including the Characean cell (Ogata and Kishimoto, 1976; Hayashi and Hirakawa, 1980; Coster et al., 1983; Hansen, 1985; Toko et al., 1988), the *Physarum plasmodium* (Ueda et al., 1987), the heart cell aggregate (Clay et al., 1984), and various biochemical reactions (Hess et al., 1975; Nicolis and Prigogine, 1977). In *Chara* too, the electrical oscillation can be elicited by electrical or physical perturbations (Boels and Hansen, 1982). It is shown in *Chara* that oscillation arises from coupling between intracellular metabolic processes and H^+-ATPase molecules (Hansen, 1985). In the present system, the oscillation seems to be intimately related to H^+-ATPase because it tended to appear in roots with larger growth speed, where absorption of nutrient may be facilitated. Those oscillations are ordered spatially and temporally. Plants show the movement as micronutation (Kristie and Jolliffe, 1986). Explication of the relationship among the electrical events found here, the nutrient absorption, and the morphogenetic change is a future task.

APPENDIX

The electrical conductances per unit length in the radial direction of the external solution, the membrane at the parenchyma/surface interface, the parenchyma symplast, and the membrane at the parenchyma/xylem interface are denoted by G_S, G_m, G_P, and G_X, respectively, in Fig. 6. Electrical resistances per unit length in the longitudinal direction of the external solution and the parenchyma are respectively denoted by R_S and R_P. Most of the electrical current flows within the cylindrical volume with a radius about five times or greater than the radius of a root (Ezaki et al., 1988). For 0.1 mM KCl and 0.05 mM $CaCl_2$ solution, therefore, R_S becomes $1.1 \times 10^5\ \Omega$/cm and G_S is $2.0 \times 10^{-4}\ \Omega^{-1}$/cm for a root of 1 mm in radius. Since the resistivity of the symplast is $\sim 2.5 \times 10^2\ \Omega$ cm (Behrens and Gradman, 1985), we obtain $R_P = 3.2 \times 10^4\ \Omega$/cm and $G_P = 6.4 \times 10^{-3}\ \Omega^{-1}$/cm. The values of G_m and G_X can be estimated to be $1.0 \times 10^{-4}\ \Omega^{-1}$/cm and $6.3 \times 10^{-7}\ \Omega^{-1}$/cm, respectively, by adopting the order of 10^{-4} in Ω^{-1}/cm^2 unit of a typical membrane. The radius of xylem was chosen as 10 μm.

The quantity as, e.g., $R_S^{(TE)}$ in Fig. 7 is given by $R_S L^{(TE)}$; hence we get $R_S^{(TE)} = 2.2 \times 10^4\ \Omega$, $R_S^{(EM)} = 8.8 \times 10^4\ \Omega$, $R_P^{(TE)} = 6.4 \times 10^3\ \Omega$ and $R_P^{(EM)} = 2.6 \times 10^4\ \Omega$ for $L^{(TE)} = 2$ mm and $L^{(EM)} = 8$ mm. Membrane electromotive forces were taken as $E_1^{(T)} = 85.5$ mV, $E_1^{(E)} = 100.5$ mV, $E_1^{(M)} = 78.7$ mV, $E_2^{(T)} = 30.7$ mV, $E_2^{(E)} = 73.8$ mV, and $E_2^{(M)} = 30.1$ mV so that the resulting surface electrical-potential pattern might agree with the observed data (Toko et al., 1989). The choice of these values did not affect the phase relation of oscillations of results, as confirmed by Eq. A10. The membrane electrical resistances as $r_1^{(T)}$ are expressed by $1/G_m L^{(T)}$; hence we obtain $r_1^{(T)} = 1.0 \times 10^5\ \Omega$, $r_1^{(E)} = 2.0 \times 10^4\ \Omega$, $r_1^{(M)} = 2.5 \times 10^4\ \Omega$, $r_2^{(T)} = 1.6 \times 10^4\ \Omega$, $r_2^{(E)} = 3.2 \times 10^3\ \Omega$, and $r_2^{(M)} = 4.0 \times 10^3\ \Omega$, whereas $r_2^{(E)}$ is changed periodically near this value. For the membrane resistances at xylem/parenchyma interface, we chose the values of 10^{-3} times those directly estimated from the above relation by taking account of insufficiency of the growing xylem structure in these regions near the root tip. The values of A and τ in Eq. 6 were chosen as $A = 1.6 \times 10^3\ \Omega$ and $\tau = 10$ min.

The steady-state propagation of electrical change is described by linear differential equations. We consider the propagation of the electrical change generated at $x = 0$ to the x-axis (Fig. A1). The equations for I_1, I_2, V_1, and V_2 indicated in Fig. A1 are:

$$\begin{aligned} \partial I_1/\partial x &= -G_1 V_1 \\ \partial (V_1 + V_2)/\partial x &= -R_S I_1 \\ \partial (I_1 + I_2)/\partial x &= -G_2 V_2 \\ \partial V_2/\partial x &= -R_P I_2, \end{aligned} \tag{A1}$$

where G_1 and G_2 are defined by

$$G_1 = G_m G_P/(G_m + G_P),\ G_2 = G_X G_P/(G_X + G_P). \tag{A2}$$

The boundary conditions are given by

$$V_1(0) = V_{10},\ V_2(0) = V_{20},\ V_1(\infty) = V_2(\infty) = 0. \tag{A3}$$

The solutions are straightforward:

$$\begin{aligned} V_1 &= C_1 \exp(-x/\lambda_1) + C_2 \exp(-x/\lambda_2) \\ V_2 &= (R_S G_1 \lambda_1^2 - 1) C_1 \exp(-x/\lambda_1) \\ &\quad + (R_S G_1 \lambda_2^2 - 1) C_2 \exp(-x/\lambda_2), \end{aligned} \tag{A4}$$

with λ_1, λ_2, C_1, and C_2 defined by

$$\begin{aligned} \lambda_1, \lambda_2 &= \{((R_S + R_P)G_1 + R_P G_2 \\ &\quad \pm \{[(R_S + R_P)G_1 + R_P G_2]^2 \\ &\quad - 4 R_S R_P G_1 G_2\}^{1/2})/2 R_S R_P G_1 G_2\}^{1/2} \\ C_1 &= [(R_S G_1 \lambda_2^2 - 1)V_{10} - V_{20}]/R_S G_1 (\lambda_2^2 - \lambda_1^2) \\ C_2 &= [V_{20} - (R_S G_1 \lambda_1^2 - 1)V_{10}]/R_S G_1 (\lambda_2^2 - \lambda_1^2), \end{aligned} \tag{A5}$$

where the minus and plus signs correspond to λ_1 and λ_2, respectively.

Because G_1 and R_S are much larger than G_2 and R_P, respectively, we obtain the approximate expressions for λ_1 and λ_2:

$$\lambda_1 = (R_S G_1)^{-1/2},\ \lambda_2 = (R_P G_2)^{-1/2}. \tag{A6}$$

This means λ_1 is much smaller than λ_2. The electrical potentials decay

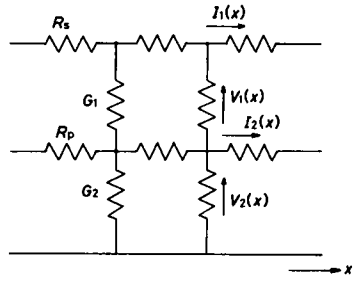

FIGURE A1 Network of longitudinal electrical resistances and radial conductances for calculating the space constant as a measure of the distance of propagation.

simply according to the approximate forms:

$$V_1 = V_{10} \exp(-x/\lambda_1),\ V_2 = V_{20} \exp(-x/\lambda_2). \quad \text{(A7)}$$

This result suggests that the propagation path can be divided into two independent ones: one is along the electrical circuit at the surface composed of G_1 and R_S, whereas the other involves the xylem/parenchyma interface composed of G_2 and R_P. The values of λ_1 and λ_2 are 3.0 and 70 mm, respectively. Thus, the electrical change along the surface-side membrane decays rapidly, but the change at the xylem/parenchyma interface can be propagated along the root.

In the external aqueous solution, the space constant is given by $(R_S G_S)^{-1/2}$, ~2 mm, which is too small for the potential change to be propagated far away from the root. Within the parenchyma symplast, the space constant is equal to $(R_P G_P)^{-1/2}$, ~0.7 mm in accord with the measurement (Behrens and Gradmann, 1985).

In Eq. 8, q, r, v_1, w_1, v_2, and w_2 are defined by

$$q = b_{11}c_{22} + b_{22}c_{11} - 2b_{12}c_{12},\ r = c_{11}c_{22} - c_{12}^2,$$
$$v_1 = d_1c_{22} + e_1b_{22} + d_2c_{12} + e_2b_{12},\ w_1 = e_1c_{22} + e_2c_{12},$$
$$v_2 = d_2c_{11} + e_2b_{11} + d_1c_{12} + e_1b_{12},\ w_2 = e_2c_{11} + e_1c_{12}, \quad \text{(A8)}$$

where b_{11}, b_{22}, b_{12}, c_{11}, c_{22}, c_{12}, d_1, d_2, e_1, and e_2 are the functions of a_{11}, a_{12}, and so on:

$$b_{11} = a_{11}(a_{33} + a_{44}) - a_{14}^2,\ b_{22} = a_{22}(a_{33} + a_{44}) - a_{23}^2,$$
$$b_{12} = a_{12}(a_{33} + a_{44}) + a_{14}a_{23},\ c_{11} = (a_{11}a_{44} - a_{14}^2)a_{33},$$
$$c_{22} = (a_{22}a_{33} - a_{23}^2)a_{44},\ c_{12} = a_{12}a_{33}a_{44},$$
$$d_1 = (a_{33} + a_{44})E_1 + a_{14}(E_3 + E_4),$$
$$d_2 = (a_{33} + a_{44})E_2 + a_{23}(E_3 + E_4),$$
$$e_1 = a_{33}(a_{44}E_1 + a_{14}E_4),\ e_2 = a_{44}(a_{33}E_2 + a_{23}E_3). \quad \text{(A9)}$$

Calculation of the ratio $\Delta i_1/\Delta i_2 = (v_1 r - w_1 q)/(v_2 r - w_2 q)$ gives

$$\begin{aligned}\Delta i_1/\Delta i_2 = -\{&[(R_P^{(TE)} + R_S^{(TE)} + r_1^{(E)} + r_1^{(T)})(R_P^{(TE)} + r_2^{(T)}) \\ &- R_P^{(TE)2}]R_P^{(EM)} - (R_P^{(EM)} + r_2^{(M)})R_P^{(TE)}r_1^{(E)}\}/ \\ &[(R_P^{(EM)} + R_S^{(EM)} + r_1^{(E)} + r_1^{(M)}) \\ &\cdot (R_P^{(EM)} + r_2^{(M)})R_P^{(TE)} \\ &- (R_P^{(TE)} + r_2^{(T)})R_P^{(EM)}r_1^{(E)} - R_P^{(EM)2}R_P^{(TE)}]. \quad \text{(A10)}\end{aligned}$$

The relaxation process must be discussed by taking account of the membrane capacitance C_x in parallel with the membrane conductance G_x. The propagation velocity v along the xylem/parenchyma interface can be approximately given by

$$v = (2\pi r_x C_x R_P t)^{-1/2}, \quad \text{(A11)}$$

with r_x denoting the radius of xylem. Eq. A11 leads to $v \sim 70.7\ t^{-1/2}$ cm/s for $C_x \sim 1\ \mu F/cm^2$. Most of the change in the electrical potential is propagated with one second or so. This is the reason why the apparent coherency is observed in the mature region.

The authors would like to express their sincere thanks to Mr. K. Hayashi and Mr. T. Fujiyoshi for valuable discussions throughout the present work.

This work was supported by grants-in-aid for Scientific Research from the Ministry of Education, Science and Culture of Japan.

Received for publication 10 April 1989 and in final form 20 October 1989.

REFERENCES

Arisz, W. H. 1956. Significance of the symplasm theory for transport across the root. *Protoplasma.* 46:5–80.

Bacic, G., and S. Ratkovic. 1984. Water exchange in plant tissue studied by proton NMR in the presence of paramagnetic centers. *Biophys. J.* 45:767–776.

Behrens, H. M., and D. Gradmann. 1985. Electrical properties of the vertically growing root tip of *Lepidium sativum* L. *Planta (Berl.).* 163:453–462.

Boels, H. D., and U.-P. Hansen. 1982. Light and electrical current stimulate same feed-back systems in *Nitella. Plant Cell Physiol.* 23:343–346.

Bowling, D. J. F. 1972. Measurements of profiles of potassium activity and electrical potential in the intact root. *Planta (Berl.).* 108:147–151.

Bowling, D. J. F. 1976. Uptake of Ions by Plant Roots. Chapman and Helle, London. Chapter 7.

Clay, J. R., M. R. Guevara, and A. Shrier. 1984. Phase resetting of the rhythmic activity of embryonic heart cell aggregates. *Biophys. J.* 45:699–714.

Coster, H. G. L., T. C. Chilcott, and K. Ogata. 1983. Fluctuations in the electrical properties of *Chara* and the spatial structure of the electrochemical characteristics. *In* Inorganic Carbon Uptake by Aquatic Photosynthesis Organisms. W. J. Lucas and J. A. Berry, editors. Waverly Press, Inc., Baltimore, MD. 255–269.

de Boer, A. H., H. B. A. Prins, and P. E. Zanstra. 1983. Bi-phasic composition of trans-root electric potential in roots of Plantago species: involvement of spatially separated electrogenic pumps. *Planta (Berl.).* 157:259–266.

Ezaki, S., K. Toko, and K. Yamafuji. 1988. Electric potential patterns around a root of the higher plant. *Trans. In. Elec. Infor. Com. Engin.* E71:965–967.

Floyd, T. L. 1989. Principles of Electric Circuits. 3rd ed. Merrill Publishing Co., Columbus, OH. Chapter 9.

Ginsburg, H., and B. Z. Ginzburg. 1974. Radial water and solute flows in roots of Zea mays. *J. Exp. Bot.* 25:28–35.

Hansen, U.-P. 1985. Messung und Interpretation der Kinetik der Lichtwirkung auf den elektrophoretischen Transport uber die Plasmamembran der Alge Nitella. *Ber. Dtsch. Bot. Ges.* 92:105–118.

Hanson, J. B. 1978. Application of the chemiosmotic hypothesis to ion transport across the root. *Plant Physiol. (Bethesda).* 62:402–405.

Hayashi, H., and K. Hirakawa. 1980. *Nitella* fluctuation and instability in the membrane potential near threshold. *Biophys. J.* 31:31–44.

Hayashi, K., K. Toko, and K. Yamafuji. 1987. Dynamic process and formation of electric pattern in bean roots. *Trans. In. Elec. Infor. Com. Engin.* J70-A:1269–1274.

Hess, B., A. Boiteux, and H. G. Busse. 1975. Spatiotemporal organization in chemical and cellular systems. *Adv. Chem. Phys.* 29:137–168.

Hodgkin, A. L., and A. F. Huxley. 1952. A quantitative description of membrane current and its application to conduction and excitation in nerve. *J. Physiol. (Lond.).* 117:500–544.

Hoffman, K. 1969. Zum Einfluß del Zeitgeberstärke auf die Phasenlage der Synchronisierten circadianen Periodik. *Z. Vgl. Physiol.* 62:93–110.

Hoppensteadt, F. C., and J. P. Keener. 1982. Phase locking of biological clock. *J. Math. Biol.* 15:339–349.

Ichino, K., K. Katou, and H. Okamoto. 1973. Distribution of electric

potential and ion transport in the hypocotyl of *Vigna sesquipedalis*. *Plant Cell Physiol.* 14:127–137.

Jenkinson, I. S., and B. I. H. Scott. 1961. Bioelectric oscillations of bean roots: further evidence for a feedback oscillator. *Aust. J. Biol. Sci.* 14:231–247.

Katou, K. 1978. Distribution of electric potential and ion transport in the hypocotyl of *Vigna sesquipedalis*. *Plant Cell Physiol.* 19:523–535.

Krinsky, V. I., and K. I. Agladze. 1983. Interaction of rotating waves in an active chemical medium. *Physica.* 8D:50–56.

Kristie, D. N., and P. A. Jolliffe. 1986. High-resolution studies of growth oscillations during stem elongation. *Can. J. Bot.* 64:2399–2405.

Nicolis, G., and I. Prigogine. 1977. Self-Organization in Nonequilibrium Systems. John S. Wiley/Interscience, New York.

Ogata, K. 1983. The water-film electrode: a new device for measuring the characean electro-potential and -conductance distributions along the length of the internode. *Plant Cell Physiol.* 24:695–703.

Ogata, K., and U. Kishimoto. 1976. Rhythmic change of membrane potential and cyclosis of *Nitella* internode. *Plant Cell Physiol.* 17:201–207.

Scott, B. I. H. 1957. Electric oscillations generated by plant roots and a possible feedback mechanism responsible for them. *Aust. J. Biol. Sci.* 10:164–179.

Spanswick, R. M. 1981. Electrogenic ion pumps. *Annu. Rev. Plant Physiol.* 32:267–289.

Toko, K., and K. Yamafuji. 1988. Spontaneous formation of the spatial pattern of electric potential in biological systems. *Ferroelectrics.* 86:269–279.

Toko, K., K. Hayashi, and K. Yamafuji. 1986. Spatio-temporal organization of electricity in biological growth. *Trans. IECE Jpn.* E69:485–487.

Toko, K., S. Iiyama, C. Tanaka, K. Hayashi, Ke. Yamafuji, and K. Yamafuji. 1987. Relation of growth process to spatial patterns of electric potential and enzyme activity in bean roots. *Biophys. Chem.* 27:39–58.

Toko, K., K. Hayashi, T. Yoshida, T. Fujiyoshi, and K. Yamafuji. 1988. Oscillations of electric spatial patterns emerging from the homogeneous state in characean cells. *Eur. Biophys. J.* 16:11–21.

Toko, K., T. Fujiyoshi, C. Tanaka, S. Iiyama, T. Yoshida, K. Hayashi, and K. Yamafuji. 1989. Growth and electric current loops in plants. *Biophys. Chem.* 33:161–176.

Ueda, T., Y. Mori, and Y. Kobatake. 1987. Patterns in the distribution of intracellular ATP concentration in relation to coordination of amoeboid cell behavior in *Physarum polycephalum*. *Exp. Cell Res.* 169:191–201.

Yoshida, T., K. Hayashi, K. Toko, and K. Yamafuji. 1988. Effect of anoxia on the spatial pattern of electric potential formed along the root. *Ann. Bot. (Lond.).* 62:497–507.